Optical Materials 121 (2021) 111550

Contents lists available at ScienceDirect

Optical Materials

journal homepage: www.elsevier.com/locate/optmat

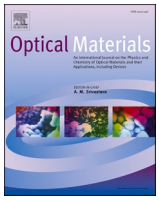

Research Article

UV light induced processes in pure and doped AlN ceramics

L. Trinkler *, A. Trukhin, J. Cipa, B. Berzina

Institute of Solid State Physics, University of Latvia, Kengaraga St. 8, Riga, LV-1063, Latvia

ARTICLE INFO

Keywords:
Aluminium nitride
UV light irradiation
Photoluminescence
Thermoluminescence
Recombination luminescence
Photoelectric effect

ABSTRACT

AlN ceramics samples, pure and doped with Y_2O_3, Eu_2O_3 and GaN, and produced from the same AlN powder, were studied for photoelectric effect, photoluminescence spectra and kinetics and thermoluminescence under irradiation with UV light from above- and below-bandgap spectral region. Common properties of all studied samples were found, such as presence of the complex UV-Blue and Red emission bands in PL and TL emission due to oxygen-related defects and manganese impurities, correspondingly; a new emission band at 320 nm, which is present in PL and absent in TL emission spectrum and is assigned to an oxygen-related centre; luminescence decay comprised of superposition of exponents of various duration from nanoseconds to hundreds of minutes. Among the studied samples the dopant-related luminescence was observed only in AlN:Eu_2O_3 at 525 nm. No effect of the dopants on fading rate of the stored TL signal was observed. Such properties of the PL and TL as luminescence intensity and relative contribution of the emission bands manifested by individual samples were explained by influence of the dopant type and ceramics sintering procedure on generation and recharging of the intrinsic and impurity defects.

1. Introduction

Aluminum nitride AlN is a wide band semiconductor (E_g = 6.2 eV) with wurtzite structure possessing a number of properties advantageous for practical application, which explains a wide interest among researchers to this material. Pure and doped AlN was studied for potential application as UV light detectors [1,2], ionizing radiation and UV light dosimeters [3–8], persistent luminophores [9] and others. AlN was studied in the form of single crystal, polycrystals, ceramics, powders and various nanostructures in order to understand the basic processes induced by different types of irradiation, particularly luminescence mechanisms, and elucidate the material's potential for practical application. Luminescence properties of AlN are determined by presence of uncontrolled impurities and intrinsic defects, the main role played by oxygen-related defects. Often the nominally pure AlN raw material contains also manganese ions in negligible number, which, however, efficiently manifest themselves in luminescence of the produced products. Doping of AlN inserts additional impurity defects into material making the process of interaction of radiation with matter ever more complicated, but in the same time arousing new useful properties and bringing new opportunities for practical application.

In our previous works [6, 7 and references therein] we have studied ceramics of nominally pure AlN. It was found that this material possesses a number of very attractive dosimeter features retrieved by TL and OSL methods, such as a higher sensitivity and large linear dynamic dose range under ionizing radiation and UV radiation, negligible influence of the heating rate on the TL response, spectral sensitivity to UV radiation close to that of human skin, TL/OSL emission in the visible spectral region, suitable for most of the light detectors and others. However, practical application of AlN dosimeter properties is hampered by high fading rate of the stored signal observed at RT, which is ascribed to tunnel recombination processes due to localised transitions between donor-acceptor pairs [10] associated with oxygen-related defects. In the present paper we study AlN ceramics with different dopants, which could diminish the fading rate of the irradiation-induced stored signal. For specific reasons the following dopants were chosen: 1) Y_2O_3, which is a good sintering aid and influences amount and distribution of oxygen impurity centres in the AlN grains during ceramics production, thus potentially affecting oxygen-related luminescence and trap centres, besides it does not manifest itself in luminescence [7]; 2) Eu_2O_3, a rare earth impurity, providing a characteristic luminescence centre in visible region and cited as a TL booster [11]; 3) GaN, proposed in small amount as an agent for the band gap engineering of AlN [12], producing AlGaN with the reduced band gap, enveloping the shallow traps responsible for the fading of the stored signal. Doping of these impurities in the AlN lattice could have effect not only on dosimetric properties of AlN, such as

* Corresponding author.
E-mail addresses: Laima.Trinklere@cfi.lu.lv, trinkler@latnet.lv (L. Trinkler).

https://doi.org/10.1016/j.optmat.2021.111550
Received 6 May 2021; Received in revised form 14 July 2021; Accepted 31 August 2021
Available online 28 September 2021

fading of the TL signal, but also on luminescence properties.

In the present paper we have tried to establish regularities of the processes induced by irradiation with UV light from the above- and below-bandgap spectral region, which are common for the pure and doped AlN ceramics, and to clear up the role of the used dopant impurities on particular manifestations of these processes in doped AlN ceramics. For this purpose the phenomena of photoelectric effect, photoluminescence and thermoluminescence observed in pure and doped AlN under irradiation with UV light, were studied.

2. Experimental

2.1. Sample preparation

AlN ceramics samples, both nominally pure and doped with Europium, Yttrium and Gallium ions, produced in various combinations and sintering conditions were studied. Here we publish results of the 5 typical samples, revealing the most intensive luminescence signal under UV light irradiation. For production of doped AlN samples AlN macro powder (20–80 μm, high purity, STREM Chemical Inc) was mixed with Y_2O_3 2 wt% (purity 99.9%, Fluka), or Eu_2O_3 (purity 99.9 Fluka) or GaN (purity 99.9, Alfa Aesar) powder using Fritsh grinding apparatus. The press form with dia 20 mm filled with powder mixture under a certain pressure was heated up to 1700 °C for 3–10 min in a spark plasma sintering apparatus SPS-825 CE, Syntex Inc. The obtained cylindrical ceramic samples were cut into 8 × 8 × 1 mm pieces for easy inserting into analysing apparatus. X-ray diffraction analyses implemented by XRD apparatus 8 Advance, Bruker AX, was used to determine ceramics phases and crystallite size, which was found around 55–65 nm for all samples. The samples with dopants contained a small amount of phases different from AlN. For the sake of convenience the samples are given short designations: P1 and P2 for pure AlN ceramics, and Y, E and G, for the AlN-Y_2O_3, AlN-Eu_2O_3 and AlN-GaN, correspondingly. The samples P1, Y, E and G are produced in similar conditions, P2 differs from P1 mainly by the pressure used. The XRD analysis has shown that amount of secondary phases in either ceramic sample does not exceed 2%. The parameters of the samples described in this study, are shown in a Table .1.

2.2. Methods and equipment

Various physical processes induced by UV light irradiation were studied for AlN ceramics samples: photoconductivity (PC), photoluminescence (PL) and thermoluminescence (TL).

2.2.1. Photoelectric effect

Photoconductivity of an insulator or a wide band semiconductor can be measured using a specific method described previously in our papers for silica and $LiGaO_2$ [13,14]. In the present study the AlN ceramic sample was attached to a holder, while a silver electrode connected sample's upper surface was connected to a dynamic capacitor electrometer VA-J-52. The photoelectric response from an electrometer was read by a voltmeter Agilent connected to a computer. Two types of excitation light sources were used: ArF (193 nm) and KrF (248 nm) lasers, with 5 mJ and 5 ns pulse, model PSX-100 (Neweks, Estonia) and a deuterium discharge lamp with MgF_2 window conjugated with interference filters or with a vacuum monochromator 0.5 m Seya-Namioka type, equipped with a spherical grating (2400 l/mm). In the case of the deuterium lamp excitation shutters were used to provide Π-shaped light pulses.

Table 1
Designations and sintering parameters of the used AlN ceramic samples.

No.	1	2	3	4	5
Designation in this paper	P1	P2	Y	E	G
Dopant; wt%	–	–	Y_2O_3; 2	Eu_2O_3; 1	GaN; 2
Sintering temperature, °C	1700	1700	1700	1700	1700
Sintering time, min	10	5	10	10	3
Sintering pressure, MPa	30	65	30	30	30
XRD phase, (secondary phase)	AlN	AlN	AlN, ($Al_5Y_3O_{12}$)	AlN, (Al_2EuO_4)	AlN, (Al_5O_6N)
Density, g/mm^3	3.17	2.81	3.26	3.20	3.04

2.2.2. Photoluminescence

Two different experimental set-ups were used for PL measurements.

1. Edinburgh Instruments spectral system with FLS1000 Spectrometer (model: FLS1000-DD-stm) equipped with CW 450 W Xenon lamp (model: Xe2) and cooled photomultiplier tube (model: R928P) for detection of luminescence signal. It was used for emission and excitation spectra measurements at room temperature.
2. Self-made set-up for PL spectral and kinetic measurements at RT and liquid nitrogen temperature (80 K), containing a mini-spectrometer Hamamatsu C10082CAH with a CCD camera. Light from a sample was collected with a toroidal mirror and focused on an optical fiber. ArF and KrF pulse lasers were used for the PL excitation. The light of lasers scattered by the sample was cut off by a filter. PL decay kinetics curves were measured with a photomultiplier tube (H6780-04) and an oscilloscope Picoscope 2208. The oscilloscope was started by luminescence signal using the sufficiently high discrimination level (~2 V), so that neither photomultiplier noise signal, nor dark current could trigger the detection start. Decay curves were recorded with PicoScope 6 program on a computer. The decay curves, as a rule, are strongly non-exponential, the decay time constants were estimated at the beginning and the end of a decay curve, taking tangent to a curve of dependence "ln (Intensity) versus time". The measured spectra as well as decay curves were smoothed using least square fit procedure.

2.2.3. Thermoluminescence

The TL measurements were done with Lexsyg Research TL/OSL reader (Freiberg Instruments, Germany) with the integrated Hamamatsu photomultiplier tube R13456, (spectral range of 185–980 nm), and integrated irradiation sources. The instrument was upgraded so as to use also UV light excitation from solid-state laser 263 nm (50 μJ, pulse duration <10 ns) through an optical fibre. Some TL measurements were done also after irradiation with the ArF laser (193 nm, 5 mJ, pulse duration 5 ns). TL glow curves were measured at heating rate of 1 K/s, up to maximum temperature of 700 K, maintaining 10 min delay after irradiation in order to decrease the afterglow influence. TL emission spectra were measured using Andor SR-303i-B spectrometer (150 lines/mm, 500 nm blaze) with DV420A-BU2 CCD camera coupled to Lexsyg TL/OSL reader with Ultra low-OH Molex optical fibre.

3. Results

Here we present results of study of physical processes induced by irradiation with UV light in five AlN ceramic samples, which differ by presence of dopants and sintering procedures: undoped (P1 and P2), and doped AlN-Y_2O_3 (Y), AlN-Eu_2O_3 (E) and AlN-GaN (G) samples. Letters in parentheses are the designations, used in this article, see Table 1. For these samples we have studied the processes of photoluminescence, including PL emission and excitation spectra and kinetics, thermoluminescence, including TL glow curves and TL emission spectra, and photoconductivity.

3.1. Photoluminescence

3.1.1. PL spectra

In our previous studies of AlN ceramics we have mentioned that typical PL emission spectra contained a broad complex UV-Blue band in the 300–550 nm region and a Red band at 600 nm [6, 7 and references therein]. Dependence on excitation wavelength allowed to distinguish constituents of the UV-blue band as the UV band at around 400 nm and the Blue band at 480 nm bands (in some publications the maxima values are slightly shifted). Origin of the 400 and 480 nm bands is connected with oxygen-related defects (V_{Al}-O_N) [15–17] and (V_{Al}-$2O_N$) [18], while the 600 nm band is ascribed to Mn^{2+} emission [19–21].

In order to make the vision of the spectra easier, PL emission spectra of each sample are given individually: Figs. 1–5 depict the normalised PL emission spectra of the samples P1, P2, Y, G, E, correspondingly. The integral spectral PL response under excitation 250 nm from the samples G: Y: P1: E: P2 varies in the proportion: 1 : 2.4: 3.1 : 3.7: 6.4.

In general, the AlN ceramic samples under investigation (except the sample E, where Eu^{2+} emission band dominates in the PL spectrum) demonstrate structure of the PL spectra, which is similar to the previously known and contains of the UV-Blue and Red bands. In the same time new spectral features and regularities have been found.

The newly discovered feature is the appearance of the 320 nm emission band, which is the best pronounced for samples P1 and G, and particularly under excitation with xenon lamp at 280 nm and ArF laser (193 nm), see Fig. 1, curves 2, 3 and Fig. 4, curves 2, 3. For the better presentation of the emission spectral structure an example of an emission curve fitting by combination of Gaussian bands is shown in Fig. 1 for the sample P1, curve 2.

PL spectra of all samples contain the subbands at 320, 400, 480 and 600 nm with different contribution yield, which determine the PL emission spectrum of a particular sample. These emission bands are characterised with the individual excitation spectra, shown in Fig. 6: the 320 nm emission is characterised with a band peaking at 280 nm, the 400 nm band has an excitation spectrum with an intensive band at 250 nm and a tail up to 360 nm, the 480 emission is excited in the main band peaking at 280 and a weak band around 350 nm, while the 600 nm emission is excited in two bands – at 260 and 400 nm.

Presence of Y_2O_3 and GaN dopants does not cause appearance of new emission bands connected with foreign impurities, see Fig. 3 for the sample Y and Fig. 4 for the sample G. In the same time AlN doping with

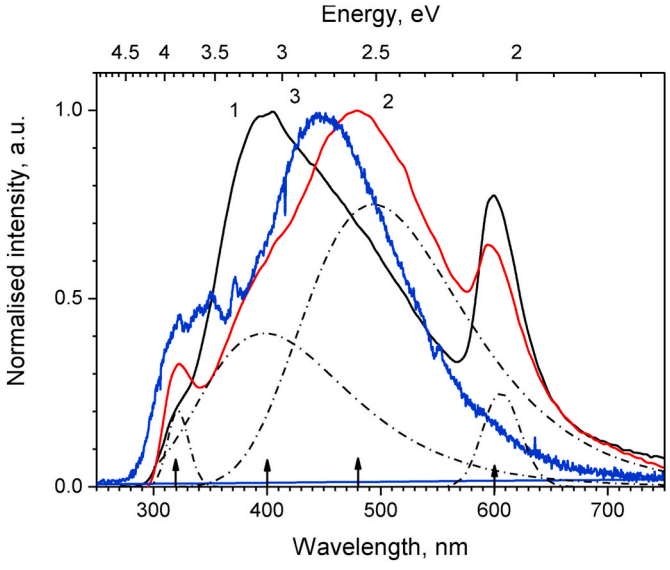

Fig. 1. PL emission spectra of P1 sample at 80 K excited with xenon lamp at 250 nm (1), 280 nm (2), and with ArF laser at 193 nm (3). Dash-dot curves show fitting of the curve (2) by Gaussian bands.

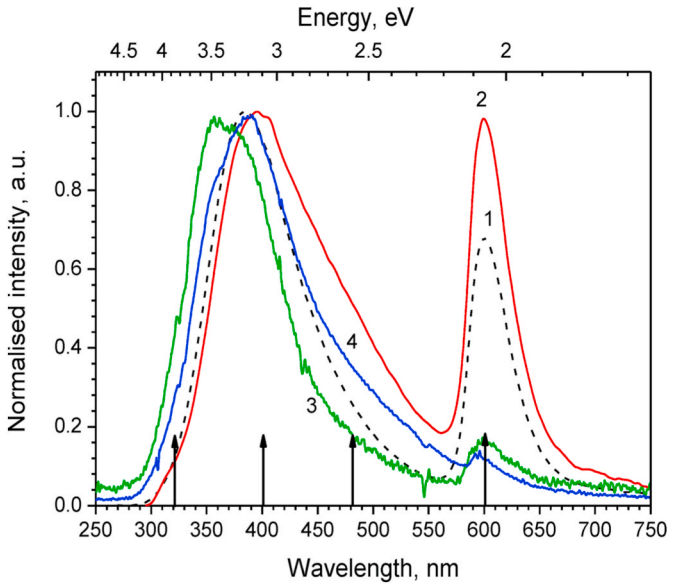

Fig. 2. PL emission of P2 sample excited with xenon lamp at 250 nm (1), 280 nm (2) and with ArF laser at 193 nm (3) at RT; and with ArF laser at 193 nm at 80 K (4).

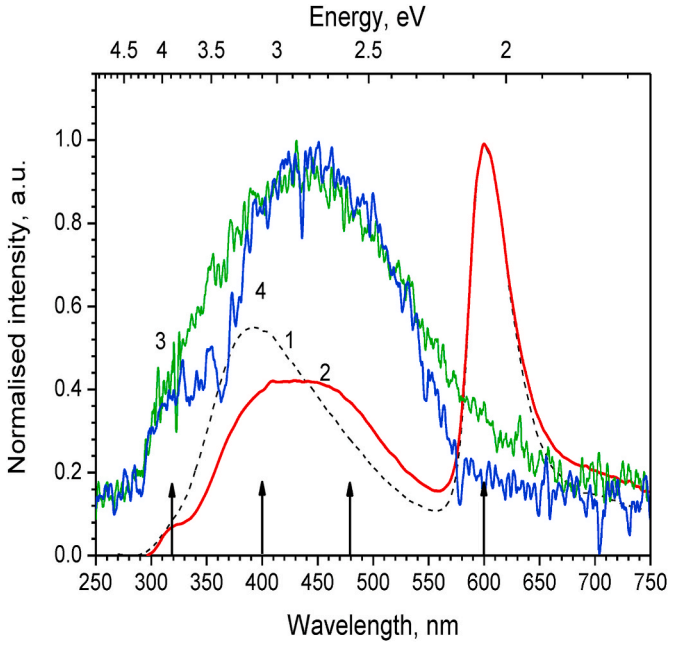

Fig. 3. PL emission of Y sample excited with xenon lamp at 250 nm (1), 280 nm (2) and with ArF laser at 193 nm (3) at RT; and with ArF laser at 193 nm at 80 K (4).

Eu_2O_3 arouses a strong band at 535 nm (see Fig. 5), assigned to Eu^{2+} emission [22,23]. It is excited in a broad band with maximum 360 nm (Fig. 6, curve 5).

Interesting effects are observed under PL excitation with the ArF laser with wavelength 193 nm, corresponding to the above band gap spectral region in AlN. In the samples with weak luminescence intensity under this type of excitation the Red band is almost not observed (P1 – Fig. 1, curve 3; Y – Fig. 3, curves 3,4; G – Fig. 4, curve 3; E – Fig. 5, curve 3), and only in the P2 sample with high luminescence intensity the 600 nm emission is well pronounced under the laser irradiation (Fig. 2, curves 3,4). On the contrary, the 320 nm band is pronounced very well under laser irradiation in the P1, Y, G and E samples, but in the P2

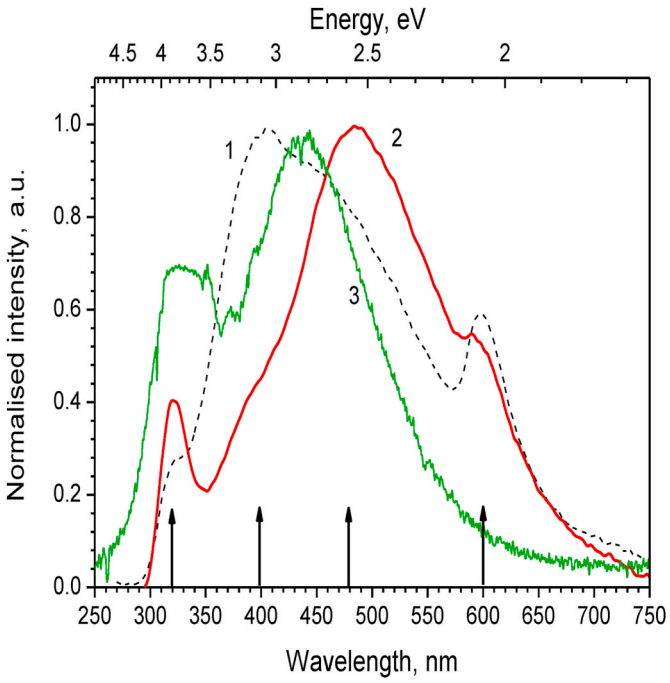

Fig. 4. PL emission of G sample excited with xenon lamp at 250 nm (1), 280 nm (2) and with ArF laser at 193 nm (3) at RT.

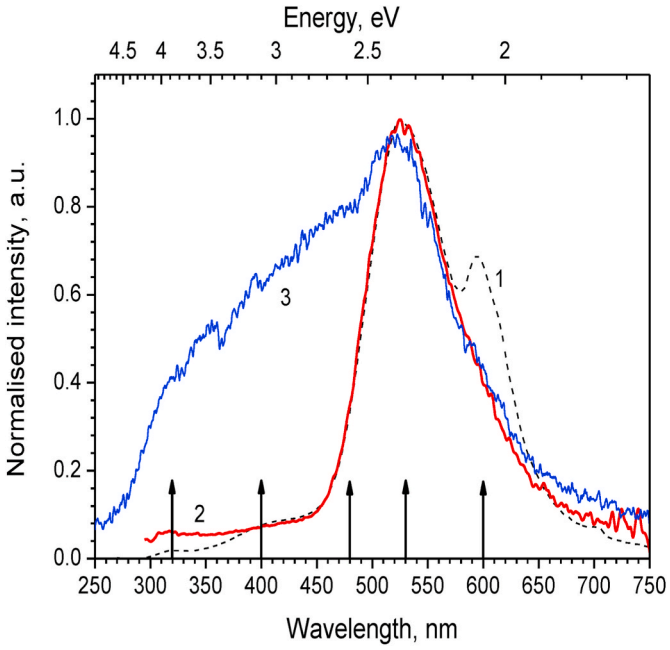

Fig. 5. PL emission of E, excited with xenon lamp at 250 nm (1), 280 nm (2) at RT and with ArF laser at 193 nm (3) at 80 K.

sample it becomes noteless due to the overlapping by the very intensive 400 nm band. In the E sample laser excitation produces both intrinsic bands 320, 400, 480 and Eu emission band 535 nm, which is dominant, and overlaps the Red band.

3.1.2. *Photoluminescence kinetics*

PL kinetics were measured for the 400 nm and 600 nm emission bands for all the studied AlN samples using pulse lasers ArF (193 nm) and KrF (248 nm) in different time ranges at RT and 80 K. For the sake of brevity a more detailed description will be given for the case of P2,

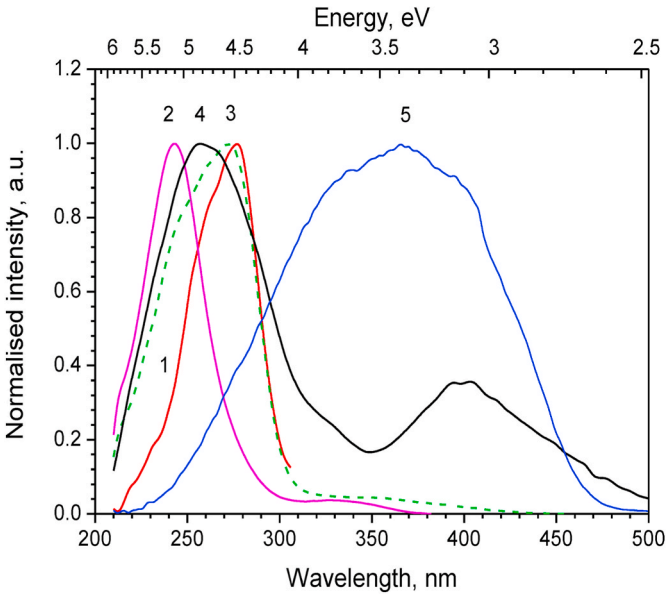

Fig. 6. Excitation spectrum at RT for selected emission wavelength (samples): 1–320 nm (P1), 2–400 nm (P2), 3–480 nm (P2), 4–600 nm (Y), 5–530 nm (E).

which is characterised with the highest PL intensity among others.

The 400 nm emission kinetics is characterised by a superposition of exponents in a broad time range - beginning from nanoseconds (not shown graphically) to minutes. Fig. 7 shows PL decay curves in the microsecond range. It is seen that the shape of the decay curves is almost the same for both excitation sources and both temperatures used, decay times can be approximated as ~0.2 μs + ~10 μs.

Fig. 8 gives PL decay curves in microsecond range for the 600 nm emission band. Here the fast component is followed by almost horizontal line, corresponding to a single exponent τ ~10 ms, especially well pronounced at RT (curves 3 and 4).

The difference between PL decay curves of the 400 and 600 nm emission bands is well seen in the millisecond range, given in Fig. 9 for excitation with the ArF laser (193 nm). The double logarithm plot shown in the insert, allows proposal that the 600 nm emission band's decay could be approximated with a single exponent $\tau \approx 10$ ms, whereas the 400 nm band's decay is characterized with a superposition of exponents.

The samples P1, Y and G possess the PL kinetic properties similar to those of the mentioned P2 sample. It is confirmed by the PL decay curves shown for the 400 nm emission band in these samples (Fig. 10) and the

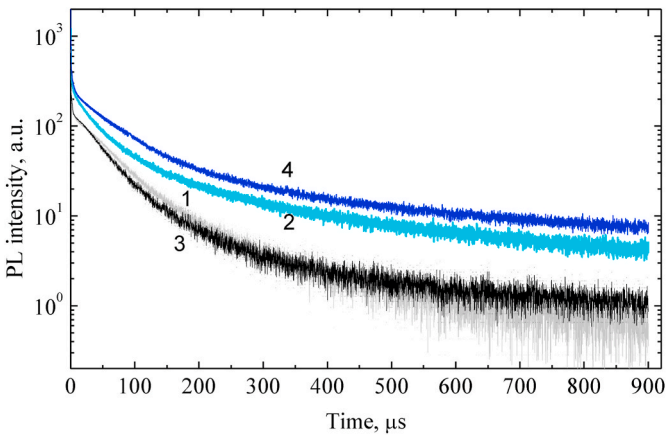

Fig. 7. P2 sample kinetics in the microsecond range of the 400 nm band under laser excitation 248 nm (1) and 193 nm (2) at 80 K; 248 nm (3) and 193 nm (4) at RT.

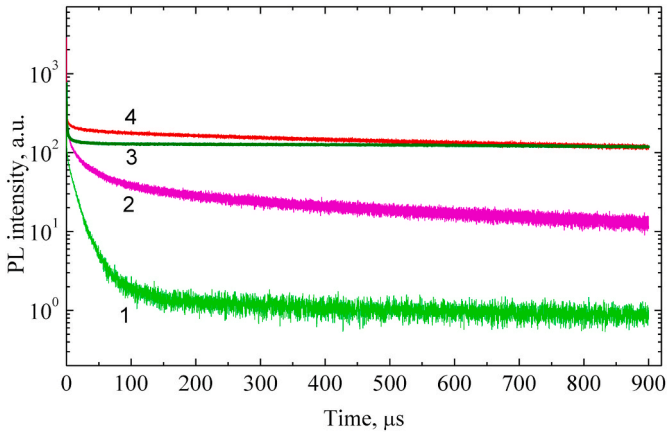

Fig. 8. P2 sample kinetics in the microsecond range of the 600 nm band under laser excitation 248 nm (1) and 193 nm (2) at 80 K; 248 nm (3) and 193 nm (4) at RT.

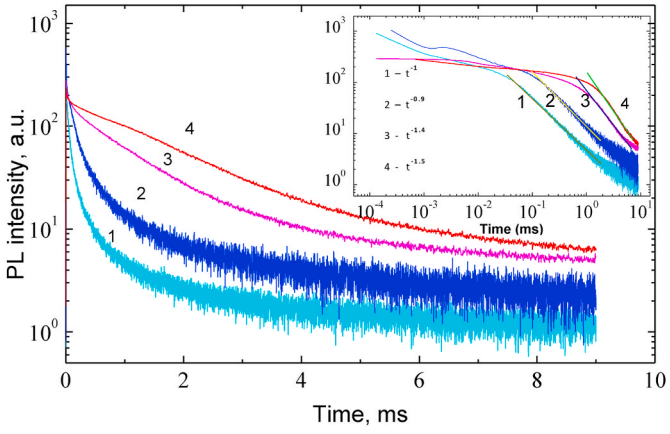

Fig. 9. P2 sample 193 nm laser excited PL kinetics in the millisecond range for luminescence 400 nm at 80 K (1); 400 nm, RT (2); 600 nm, 80 K (3); 600 nm, RT (4). Insert – the same dependences in the double logarithm plot.

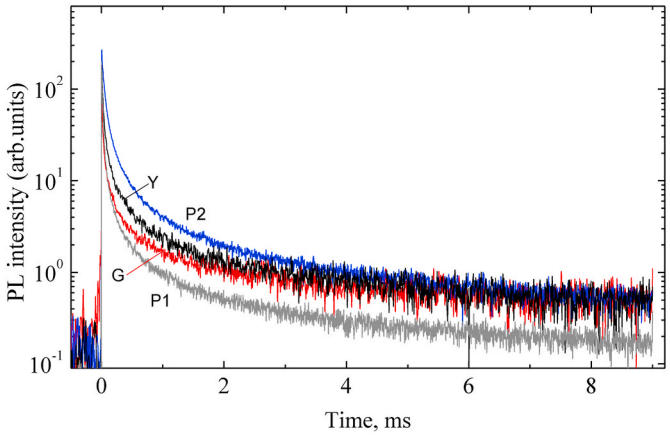

Fig. 10. PL kinetics of the emission band 400 nm of the samples P1, P2, Y and G at 80 K, excited with the 193 nm laser (193 nm).

600 nm band (Fig. 11), obtained under irradiation with the 193 nm laser at 80 K. Here we should remind that in the P1, Y and G samples the Red band is very weak and overlapped by the UV-Blue band, that is why the decay curves do not follow strictly the behaviour of the 600 nm band of the P2 sample.

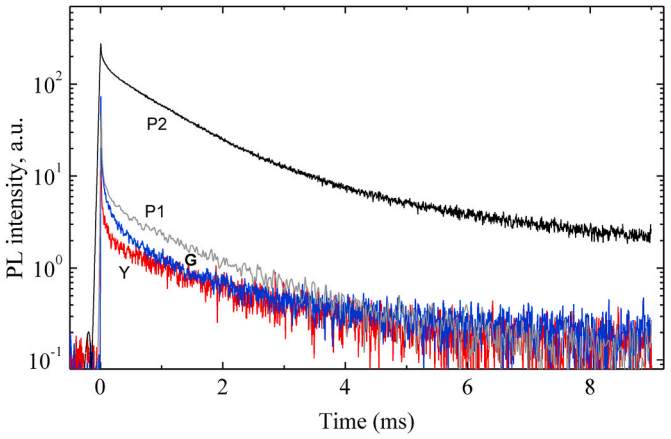

Fig. 11. Kinetics of the emission band 600 nm of the samples P1, P2, Y and G at 80 K, excited with the 193 nm laser (193 nm).

In the sample E, decay kinetics was measured in the well pronounced emission band 525 nm, assigned to Eu^{2+} 5d-4f transition [11] under excitation with the 193 and 248 nm lasers at 80 K. From Fig. 12 it is seen that PL decay is faster under 193 nm excitation compared to that of 248 nm. Estimated superposition of decay constants in the mentioned time scales is 0.1 μs + 5 μs +100 μs + 7 ms versus 0.3 μs + 7 μs + 150 μs + 24 ms, under the 193 nm and 248 nm lasers irradiation, correspondingly.

3.2. Thermoluminescence

The thermoluminescence response of the samples P1, P2, Y, G and E to UV light irradiation was measured after dosing with the lasers 193 nm and 263 nm in the similar experimental conditions. TL glow curves and TL emission spectra were measured.

Tl glow curves obtained after irradiation with the ArF laser (193 nm), Fig. 13, and the solid state laser (263 nm), Fig. 14 are similar, with slight variations in curve shape and relative yield of individual samples. In both cases the thermal glow curves have peaks around 390 K. This result is similar to our previous TL measurements of AlN-Y_2O_3 ceramics, where after 240–250 nm irradiation TL peak was observed around 370 K; while irradiation at 350 nm gave TL curve maximum at 550 K [5]. Recently similar TL curves peaking at around 350 K were obtained in AlN microcrystals after UV irradiation at 260 nm [24]. From the TL glows curves it is seen that doping with Y_2O_3, Eu_2O_3, GaN gives no sufficient effect on shifting of the TL glow peak to higher temperatures, that means that fading of the UV-light induced stored TL signal has not improved.

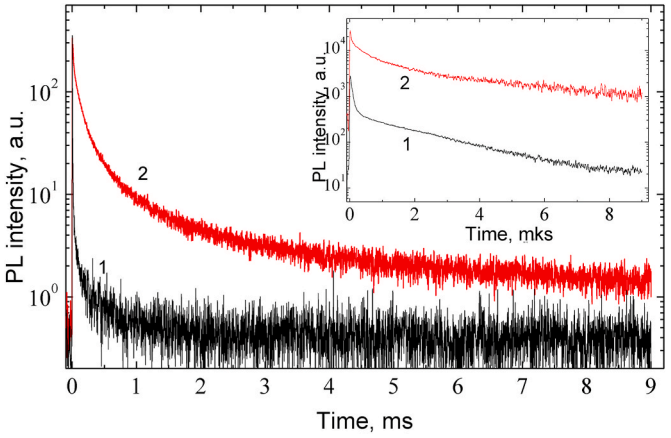

Fig. 12. Kinetics of 535 nm band of the E sample in millisecond range at 80 K, excited with lasers 193 nm (1) and 248 nm (2). Insert: the same dependences in microsecond range.

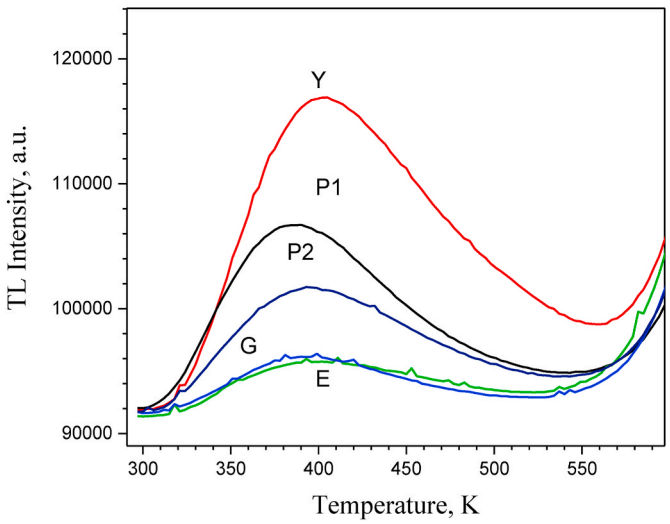

Fig. 13. TL glow curves of the P1, P2, Y, G and E samples after irradiation with the 193 nm laser, taken for the integral emission 300–700 nm, irradiation and delay time 10 min.

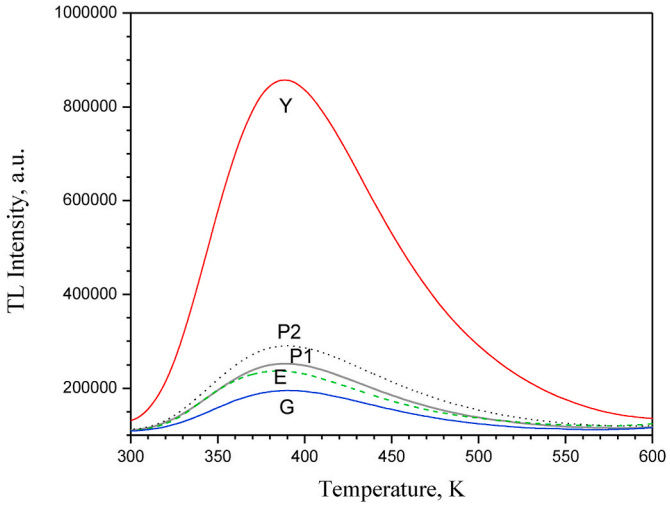

Fig. 14. TL glow curves of the P1, P2, Y, G and E samples after irradiation with the 263 nm laser, taken for the integral emission 300–700 nm, irradiation 60 s, delay 10 min.

In general, the TL emission spectra after laser irradiation 193 nm (Fig. 15) and 263 nm (Fig. 16) are similar; they consist of the broad UV-Blue and Red emission bands. The UV-Blue band is composed of the 400 and 480 nm subbands, whereas no evidence of the 320 nm subband contribution is seen at either irradiation wavelength. It is proved by fitting with combination of Gaussian bands, shown in Fig. 16 for the TL emission of the sample Y. In the TL emission spectra induced by irradiation with 193 nm, the relative contribution of the Red band is larger than in the case of irradiation with the 263 nm laser. Presence of a very weak Eu^{2+} ion emission in the E sample determines the slight red shift of the UV-Blue bands peak in the TL emission spectrum, see Fig. 15. In the paper [11] TL emission spectrum from AlN:Eu_2O_3, also contained only the intrinsic luminescence bands, while europium emission was negligible.

The largest TL response is obtained from the sample Y, which outperforms by several times the signal from other samples under the same irradiation/reading conditions, whereas in PL the most intensive luminescence signal was obtained from the sample P2.

Comparing contribution of the 400 and 600 nm bands to the

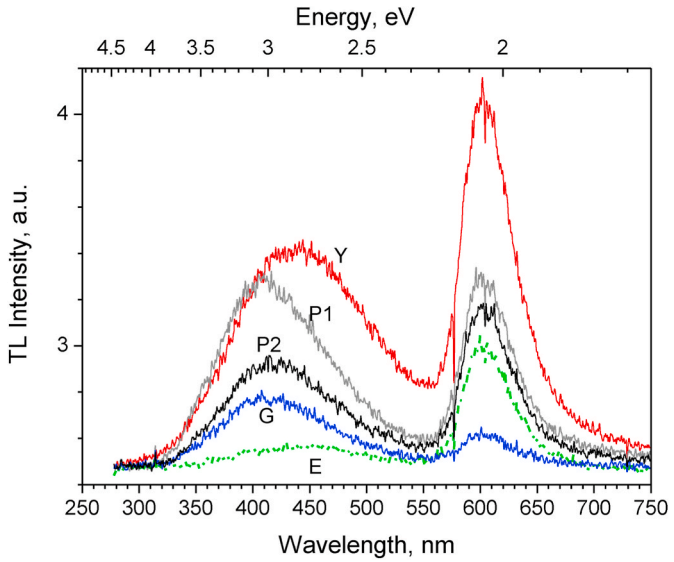

Fig. 15. TL emission spectra of the P1, P2, Y, G and E samples after irradiation with the 193 nm laser, taken at 390 K, irradiation and delay time 10 min.

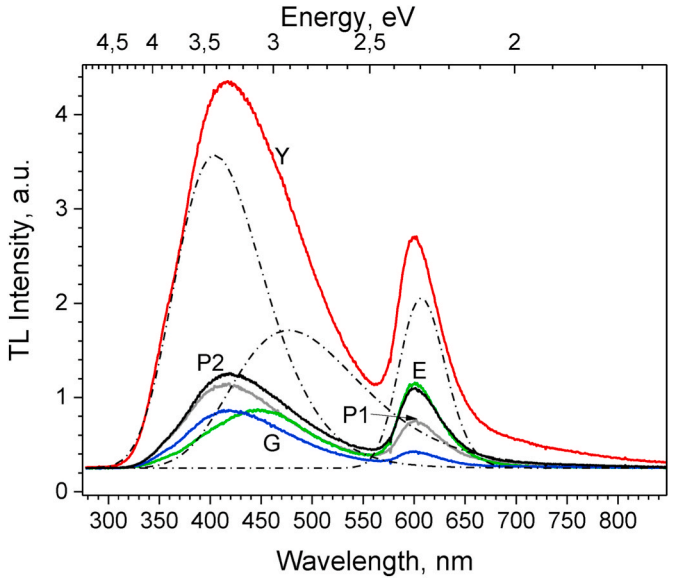

Fig. 16. TL emission spectra of the P1, P2, Y, G and E samples after irradiation with the 263 nm laser, taken at 390 K, irradiation 60 s, delay 10 min. Dash-dot curves show fitting of the curve Y by Gaussian bands.

emission spectra under the above- and below-band gap excitations for the studies samples, the difference can be seen in the PL and TL cases, moreover, it varies with the samples studied. The example of the Y sample is the most illustrative: in the PL emission spectrum (Fig. 3) the Red band is dominant under 250 and 280 nm excitation, and negligibly small under 193 nm excitation; on the contrary, in the TL emission spectrum the contribution of the Red band is dominant compared to the 400 nm band after 193 nm irradiation (Fig. 15), and is much smaller after 263 nm irradiation (Fig. 16).

3.3. Photoconductivity

We have found that the studied samples demonstrate the photoconductivity under irradiation with UV light. Fig. 17 shows the photoelectric signal under the Π shape irradiation with the 193 nm laser for the samples P1, G and Y. During irradiation the photoelectric signal

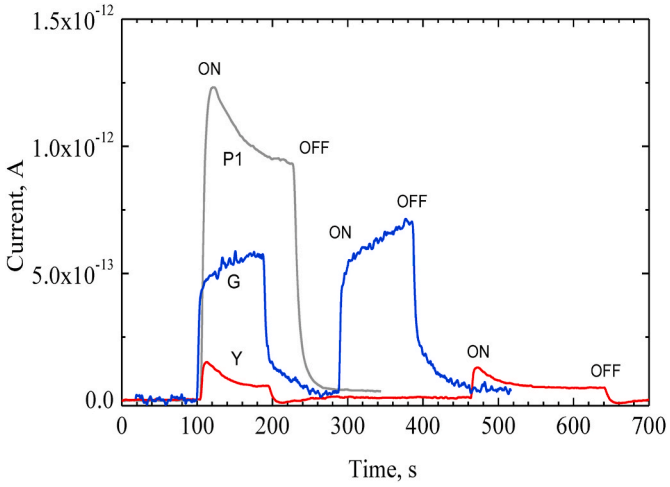

Fig. 17. Photocurrent signal under irradiation with the ArF (193 nm) laser for the P1, G and Y samples. Start/End of irradiation is shown by ON/OFF.

either decreases (P1 and Y) or increases (G). After ceasing of irradiation the photoelectric signal decreases with a slow relaxation time, which takes hundreds of seconds. The same phenomenon was observed also for other samples.

By means of the example of the G sample (Fig. 18) it is shown, that photoelectric signal is aroused by different UV wavelengths, including the above-band gap region (193 nm, or 6.42 eV), band edge (200 nm, or 6.2 eV), and below-band gap region (254 nm, or 4.88 eV), the latter corresponding to defect excitation. Since different light sources were used for illumination, the intensity of the signals cannot be compared. Similarly, in all studied pure and doped AlN ceramic samples the photoelectric effect is observed under illumination with UV light corresponding to above- and below-bandgap spectral region.

4. Discussion

In the present paper the specific dopants of AlN ceramics: Y_2O_3, Eu_2O_3, GaN were used in order to study their influence on the fading rate of the UV-light induced TL signal. The TL glow curve characteristic for pure AlN ceramics after irradiation with 193 or 263 nm, begins at RT and peaks at about 390 K. Such low-temperature position of the TL glow peak facilitates the uncontrolled fading of the stored TL signal. If introduction of impurity ions could shift the peak position to higher

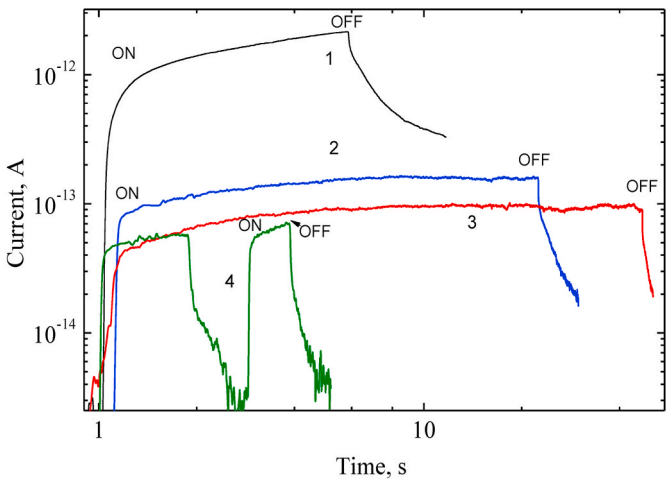

Fig. 18. Photocurrent signal in the sample G under irradiation with lasers: 193 nm (1), 248 nm (2); and deuterium lamp with interference filters 200 nm (3), 254 nm (4). Start/End of irradiation is shown by ON/OFF.

temperatures, the TL signal would become more stable during storage time. Though the essential change of the TL curves, and hence, improvement of the dosimetric properties were not obtained, the experimental results presented above allow judge about the physical processes occurring in AlN ceramics samples under UV radiation and about the role of the dopants in their manifestation.

In this study we have used UV light sources with wavelengths, matching the above-bandgap region (ArF laser 193 nm, or 6.43 eV) and below-bandgap spectral region (KrF laser 248 nm, or 5 eV; solid state laser 263 nm, or 4.71 eV, as well as UV lamps with filters or a monochromator). We have confirmed that in all studied AlN ceramics samples irradiation with UV light in the above-band gap spectral region produces free charge carriers, which are responsible for photocurrent, recombination photoluminescence, and are trapped at the trap centres, thermal release from which gives thermoluminescence. UV light irradiation with the below-band gap energies, corresponding to absorption of defects, arouses luminescence of the defect centres and their ionization, providing free charge carriers, which in their turn also determine PC, PL and TL. Let us discuss in details the novel aspects of the processes induced in doped AlN ceramics under UV irradiation.

4.1. Photoconductivity

AlN is a wide band gap material with good insulating properties and a high breakdown field. Photoconductivity has been observed in this material, when it is in the form of thin films [25] or nanowires [26,27] and illuminated with below-band gap wavelengths. In the case of high quality defect-free AlN nanowires [28] the photoelectric effect was observed under the above-band gap illumination (193 nm laser) with a sharp cutoff of the response at 208 nm. To our best knowledge, in the present work for the first time we have demonstrated a photoelectric effect occurring in pure and doped AlN ceramics under irradiation with light from both above- and below-bandgap region, arousing band-to-band transitions, and ionization of the defect centres, correspondingly, both processes providing appearance of free charge carriers in material. Study of the photoconductivity in AlN ceramics is at the initial stage and needs additional efforts, which will show the effect of particular dopants on parameters of the photoeffect.

4.2. Nature of the luminescence centres and luminescence mechanisms

In our previous paper we have proposed that the broad UV-Blue band, observed in PL, afterglow and TL emission spectra of AlN ceramics is mainly due to tunnel recombination in two types of donor-acceptor pairs: $(V_{Al}\text{-}O_N) + O_N$ and $(V_{Al}\text{-}2O_N) + NN$ (unknown donor), providing the 400 and 480 nm emission subbands, correspondingly [7, 10 and references therein]. The charging state of the oxygen-related centres was not specified. According to Ref. [24] charge carrier trapping centres are based on nitrogen vacancies V_N. Positions of the luminescence subbands are not strictly fixed, they depend on form of AlN – thin film, nanostructure or powder, on concentration of the oxygen in the sample [15,16], and on the intensity of the excitation light [10]. Besides, presence of luminescence bands of other centres in the same spectral region is also possible. Thus, luminescence of F-center type defects based on V_N in AlN nanopowder was reported in Ref. [29]. The abundance of possible luminescence centres in UV-Blue range in AlN and their variable position makes the interpretation complicated.

The authors of the recent paper [30] proposed the possibility of thermal equilibrium coexistence of two different charging states of oxygen-related defects $(V_{Al}\text{-}O_N)^{2-}$ and $(V_{Al}\text{-}O_N)^{1-}$; $(V_{Al}\text{-}2O_N)^{1-}$ and $(V_{Al}\text{-}2O_N)^0$. In the same time one of the centres - $(V_{Al}\text{-}2O_N)^0$ with the predicted luminescence around 4.0 eV (310 nm) was not found experimentally.

In the present work we report about the newly found 320 nm emission band in pure and doped AlN ceramics. Similar emission band at 320 nm under 280 nm excitation was found also in AlN: SrF_2 ceramics

[31], and assigned by the authors to Sr-induced defects. However, presence of the 320 nm emission in pure and doped with various impurities AlN ceramics speaks in favour of the intrinsic nature of this band. In terms of the concept of coexistence of two different charging states of oxygen-related defects and basing on the above mentioned experimental results, we propose the interpretation of the newly found emission band at 320 nm (3.87 eV), as the emission from $(V_{Al}\text{-}2O_N)^0$ center, whereas the 480 nm subband, as before, is ascribed to $(V_{Al}\text{-}2O_N)$ with a specified charging state $^{(1\text{-})}$: $(V_{Al}\text{-}2O_N)^{1\text{-}}$. The following experimental facts support this idea: 1) the 320 emission band occurs under excitation with light from the above-bandgap region and at the 280 nm (Fig. 1, curves 3,4,5), which coincides with the excitation of the 480 nm band (Fig. 6); 2) the 320 nm band is not observed in TL emission spectra (Figs. 17 and 18). These facts can be explained by recharging of some of the $(V_{Al}\text{-}2O_N)$ centres from the (−1) to (0) state during appearance of electron-hole pairs under band-to-band irradiation and during ionization process under 280 nm excitation. The reverse recharging process from (0) to (−1) state occurs during heating and release of the trapped charge carriers, destroying the $(V_{Al}\text{-}2O_N)^0$ centres, which, as a result, are absent in the TL emission. As for the $(V_{Al}\text{-}O_N)$ centres, responsible for the 400 nm subband in AlN ceramics, their charging state remains unknown at the present moment.

The mechanism of luminescence, responsible for the 400 nm band, was proposed in Refs. [7,10], as radiative tunnel recombination of the donor-acceptor pairs (DAP) with random separation distance, where $(V_{Al}\text{-}O_N)$ after ionization plays the role of acceptor, and O_N with a captured electron on it serves as a donor. The tunnelling probability is inversely proportional to DAP separation distance, the closer pairs recombine faster, the more distant – more slowly. This concept explained properties of the 400 nm band revealed in PL (blue shift of the peak with increase of the excitation density), afterglow (red shift with delay time) and TL (red shift with temperature rise). Luminescence decay of such process should be comprised of superposition of exponents, corresponding to the set of DAP separation distances.

Indeed, our present measurements show, that the 400 nm band's decay constants vary from a very fast component, which is not longer than several nanoseconds, up to very slow components, manifesting themselves in the afterglow and lasting up to hundreds of minutes. Similar observation of AlN decay times are found in literature: the PL fast decay components in the range of nanoseconds were observed in Refs. [32,33], while the slow afterglow decay constant about 600 s was detected also in Ref. [34]. The present PL decay kinetics measurements involve microsecond and millisecond scale. The complicated non-exponential (or exponent superposition) luminescence decay of the sample P2 is seen under the 193 and 248 nm pulse excitation, both at RT and 80 K in millisecond range (Figs. 7 and 9). In the insert of Fig. 9 the double logarithm plot is shown together with the decay fitting constituting t^{-1} and $t^{-0.9}$ for the ArF laser excited 400 nm emission at 80 K and RT, correspondingly. According to Ref. [35] the luminescence decay law with exponents ranging from −0.95 to −1.5 is typical for tunnel recombination of partner centres with random distribution. PL decay kinetics, measured for P1, Y and G samples practically coincides with that of P2, as it is seen from Fig. 10. Presence of dopants in AlN does not influence behaviour of the luminescence decay. In general, the PL kinetics obtained confirms the concept of the 400 nm band as arising from radiative tunnelling of DAP with random separation distances.

The Red emission centered at 600 nm is another band, usually present in AlN materials, which are produced from the commercial powder. It arouses from the $^4T_1(^4G) \rightarrow {}^6A_1(^6S)$ transitions of Mn^{2+} ion [9], present in AlN as uncontrolled impurity in negligible concentration. Luminescence decay of this band also contains components of different duration, beginning from nanoseconds and lasting for hours. Very slow red luminescence, demonstrated by AlN:Mn allows proposal of this material as a red persistent luminescence phosphor for practical applications [9]. An example of the decay constant in the intermediate time scale was presented by Ref. [36] as $\tau = 1.18$ ms. Our results also showed a set of different components in Mn luminescence decay, among them, however, decay curves in 1 ms scale deserve a special attention (see Fig. 8), where 600 nm emission decay curves under the 193 and 248 nm excitation at RT and 80 K after initial fast component are presented with almost horizontal lines, approximately estimated by a single exponent $\tau \approx 10$ ms. In Fig. 9 and its insert the difference in behaviour with the 400 nm band is seen. The 600 nm curves' tails are approximated by $t^{-1.4}$ (at 80 K) and $t^{-1.5}$ (at RT) law. Such power coefficients also correspond to the tunnel recombination behaviour [34]. We propose that in the time scale up to 10 ms the Red luminescence decay corresponds to intracenter transitions. Longer components of luminescence decay are determined by the delayed excitation of manganese ions either by low probability of tunnelling recombination with a distant partner (similarly to the 400 nm band), or isothermally stimulated luminescence. The final stage of the Red luminescence recombination process, of whatever duration, always ends with the intracenter luminescence, as it is confirmed by the luminescence afterglow spectra, never changing its shape with the delay time, contrary to the 400 nm band, which demonstrates a red shift [7].

Intensity of the Red emission band in P2, Y and G samples excited by the 193 nm laser is low, but still it is seen that the corresponding decay curves are similar to that of the P1 sample (Fig. 11).

The sample E, AlN:Eu_2O_3, is the only one among the studied samples, where dopant ion provides its own luminescence. According to literature, PL from AlN:Eu should demonstrate 5d-4f transitions of Eu^{2+} (520 nm), $^5D_0 \rightarrow {}^7F_2$ (610 nm) - transitions of Eu^{3+} and $^5D_0 \rightarrow {}^7F_4$ (700 nm) - transitions of Eu^{3+} [11]. In our sample we observe only the 525 nm band due to Eu^{2+}, while the weak Eu^{3+} bands are not resolved, probably, due to overlapping with the manganese-induced Red emission band (Fig. 5). The 525 nm emission is excited in a broad excitation band centered at 360 nm (Fig. 6) and also in the above band gap spectral region. Kinetics of the 525 nm band was measured at 80 K under excitation with the lasers 193 and 248 nm in the microsecond and millisecond time scales (Fig. 12 and insert therein). It is seen that luminescence decay is faster under the 193 nm excitation than under the 248 nm excitation, and both curves are nonexponential. KrF laser wavelength 248 nm hits the tail of the Eu^{2+} excitation band (230–470 nm), and in the same time corresponds to excitation of the 400 nm emission band, which could be reabsorbed, due to overlapping with the broad Eu^{2+} excitation band. The reabsorption of the 400 nm emission excited by the 248 nm laser, may be the cause of the delayed luminescence compared with that excited by electron-hole pairs produced by the 193 nm laser. Similarly to the 400 and 600 nm bands luminescence emission from Eu^{2+} at 525 nm also obtains persistent character at longer decay times.

Though all the studied AlN ceramics samples are produced from the same raw material, their luminescence properties, such as the PL and TL intensity and mutual relation of the emission bands vary from sample to sample. This observation refers also to the pure AlN samples P1 and P2, which have the same composition but distinguish in sintering procedure: PL intensity of P2 is twice as large as that of P1, mostly on the account of the larger 400 nm emission band and the better pronounced 600 nm band. The samples P1, Y, G and E are sintered according to the same identical procedure and distinguish in impurity additives.

Doping with Eu_2O_3 provides appearance of the impurity emission (Eu^{2+} gives 525 nm band), which is very strong in PL and weak in TL emission spectra. No additional features are observed in the TL glow curves, that means that no additional trapping centres are generated by doping of this impurity.

Adding of Ga impurity even in a small amount (2 wt%) strongly suppresses the PL and TL intensity. Analogous effect was observed in Ref. [37], where doping of γ-Al_2O_3 with Ga reduced luminescence of CH defect centre by several times. Authors explained this effect by appearance of characteristic gallium level near the bottom of the conduction band, thus reducing the band gap and overlapping with the excited state level of the luminescence centre. Similarly, in AlN adding of Ga ions could have caused reduction of the band gap and overlapping with the excited state of the oxygen-related luminescence centre,

responsible for the 400 nm band. No effect on the charge carriers trapping levels was observed.

Yttrium impurity provides the highest TL intensity among other samples. The favourable role of Y_2O_3 in homogenous distribution of the oxygen centres in AlN micrograins during sintering of AlN ceramics was observed in early publications [7, and references therein]. Isolated grains of secondary phase of $Al_5Y_3O_{12}$ are formed, draining the excess oxygen from AlN grains. Yttrium containing grains do not participate directly in PL and TL, all luminescence processes take place in AlN grains.

We may conclude that both sintering procedure and doping of the AlN ceramics influence generation of the oxygen-related centres of various types as well as their charging states, manifested as 320, 400 and 480 nm emission bands. Concentration of manganese ions is the same in all the studied samples; however intensity of the manganese-related Red band in PL and TL emission spectra differs. It implies that charging state of the manganese ions are also affected by sintering procedure and doping character.

5. Conclusions

In the present study we have investigated several AlN ceramics, produced from the same AlN powder, both pure and doped with Y_2O_3, Eu_2O_3 and GaN. Photoluminescence spectra and kinetics, thermoluminescence and phoconductivity under the above- and below-band gap excitations were studied. The main conclusions may be summarized as following:

1. In pure and doped AlN ceramics a photoelectric effect is observed under irradiation with UV light from the above- and below-bandgap spectral regions, confirming generation of free charge carriers.
2. In all samples the photoluminescence and thermoluminescence emission spectra contain the complex UV-Blue band, consisted mainly of 400 and 480 nm subbands, assigned to recombination luminescence with participation of oxygen-related centres, and the Red band peaking at 600 nm, assigned to uncontrolled manganese impurities. In the AlN:Eu_2O_3 sample an additional band at 525 nm is observed due to Eu^{2+} radiative transitions.
3. In all samples a novel band at 320 nm is found, which is present in PL under the 193 and 280 nm excitation, and is absent in TL. It is preliminary ascribed to recombination luminescence with participation of $(V_{Al}\text{-}2O_N)^0$ centres.
4. In all samples photoluminescence kinetics shows that emission of all luminescence bands has a complicated behaviour, characterized by superposition of exponents of different duration, varied from nanoseconds to hundreds of minutes. The set of varied time constants is determined by probability of tunnel recombination with partner centres at different separation distance and by recombination with charge carriers isothermally liberated from the traps.

Decay characteristics of the 400 nm band confirm the concept of the tunnel recombination of the donor-acceptor pair with random distribution of separation distance. Analysis of the 600 nm band's behaviour allows proposal that in the microsecond time scale luminescence decay is determined by Mn^{2+} intracenter transitions, while at longer time scales the tunnel recombination processes are determinant. Basing on decay characteristics of Eu^{2+} emission an assumption is done concerning the 400 nm emission reabsorption by the europium ion under the 248 nm excitation.

5. The differences in the PL and TL intensities and relative contribution of the UV-Blue and Red bands observed in the studied samples are explained by influence of sintering procedure and doping impurities on generation of the oxygen-related centres of various types and charging state of intrinsic and impurity defects. No effect of the used dopants on the TL glow curve peak, and hence on the TL signal fading rate, was observed.

CRediT authorship contribution statement

L. Trinkler: Conceptualization, Writing – original draft, Supervision, Project administration. **A. Trukhin:** Methodology, Investigation. **J. Cipa:** Methodology, Investigation. **B. Berzina:** Writing – review & editing, Supervision.

Declaration of competing interest

The authors declare that they have no known competing financial interests or personal relationships that could have appeared to influence the work reported in this paper.

Acknowledgments

The present research has been sponsored by the Latvian Council of Science, Grant No. lzp-2018/1-0361 "Research of luminescence mechanisms and dosimeter properties in prospective nitrides and oxides using TL and OSL methods ".

Institute of Solid State Physics, University of Latvia as the Center of Excellence has received funding from the European Union's Horizon 2020 Framework Programme H2020-WIDESPREAD-01-2016-2017-TeamingPhase2 under grant agreement No.73950, project CAMART^2

References

[1] J. Li, Z.Y. Fan, R. Dahal, M. L Nakarmi, J.Y. Lin, H.X. Jiang, 200 nm deep ultraviolet photodetectors based on AlN, Appl. Phys. Lett. 89 (2006), 213510, https://doi.org/10.1063/1.2397021.

[2] Y.A. Ali, K. Teker, Fabrication of ultraviolet photodetector with aluminum nitride nanowire networks via direct transfer method, Microelectron. Eng. 211 (2019) 26–28, https://doi.org/10.1016/j.mee.2019.03.016.

[3] L. Trinkler, L. Botter-Jensen, P. Christensen, B. Berzina, Stimulated luminescence of AlN ceramics induced by ultraviolet radiation, Radiat. Meas. 33 (2001) 731–735, https://doi.org/10.1016/S1350-4487(01)00093-2.

[4] L. Trinkler, L. Boetter-Jensen, B. Berzina, Aluminium nitrate ceramics: a potential UV dosemeter material, Radiat. Protect. Dosim. 100 (N 1–4) (2002) 313–316, https://doi.org/10.1093/oxfordjournals.rpd.a005876.

[5] L. Trinkler, B. Berzina, A. Auzina, M. Benabdesselam, P. Iacconi, UV light energy storage and thermoluminescence in AlN ceramics, Phys. Stat. Sol.(c) 4 (No.3) (2007) 1032–1035, https://doi.org/10.1016/j.nima.2007.05.177.

[6] L. Trinkler, B. Berzina, Luminescence properties in AlN ceramics and its potential application for solid state dosimetry, in: In Book: Advances in Ceramics – Characterization, Raw Materials, Processing, Properties, Degradation and Healing, Publisher: InTech, 2011, pp. 59–82, https://doi.org/10.5772/18658, 59-82.

[7] L. Trinkler, B. Berzina, E. Palcevskis, AlN Ceramics from nanosized plazma processed powder, its properties and application, in: Book: Nitride Ceramics. Combustion Synthesis, Properties and Applications, Wiley-VCH, 2014, pp. 265–293, https://doi.org/10.1002/9783527684533.ch9.

[8] J. Cipa, L. Trinkler, B. Berzina, Thermoluminescence response of AlN:t2O3 to the Sun and X-ray irradiation, Latv. J. Phys. Tech. Sci. N1 (2021) 3–14, https://doi.org/10.2478/lpts-2021-0001.

[9] J. Xu, N.J. Cherepy, J. Ueda, S. Tanabe, Red persistent luminescence in rare earth-free AlN:Mn2+ phosphor, Mater. Lett. 206 (2017) 175–177, https://doi.org/10.1016/j.matlet.2017.07.015.

[10] L. Trinkler, B. Berzina, Localised transitions in luminescence of AlN ceramics, Radiat. Meas. 71 (2014) 232–236, https://doi.org/10.1016/j.radmeas.2014.02.016.

[11] Y. Onoda, T. Kato, K. Fukuda, N. Kawaguchi, T. Yangida, Thermally stimulated luminescence properties of Eu-doped AlN ceramic, Optik 181 (2019) 50–56, https://doi.org/10.1016/j.ijleo.2018.11.160.

[12] M. Fasoli, A. Vedda, M. Nikl, C. Jiang, B.P. Uberuaga, D.A. Andersson, K. J. McClellan, C.R. Stanek, Band-gap engineering for removing shallow traps in rare-earth Lu3Al5O12 garnet scintillators using Ga3+doping, Phys. Rev. B-Condens. Matter Phys. 84 (2011) 1–4, https://doi.org/10.1103/PhysRevB.84.081102.

[13] A. Trukhin, Investigation of the photoelectric and photoluminescent properties of crystalline quartz and vitreous silica in fundamental absorption region. Model for electronic structure and migration of energy in SiO2, Phys. Stat. Sol.(b) 86 (1978) 67–75, https://doi.org/10.1002/pssb.2220860107.

[14] A. Trukhin, L. Trinkler, Photoconductivity and photoelectron emission of $LiGaO_2$ crystal excited in intrinsic absorption range, Opt. Mater. 93 (2019) 11–14, https://doi.org/10.1016/j.optmat.2019.05.005.

[15] G.A.J. Slack, Nonmetallic crystals with high thermal conductivity, J. Phys. Chem. Solid. 34 (1973) 321–335, https://doi.org/10.1016/0022-3697(73)90092-9.
[16] R.A. Youngman, J.H. Harris, Luminescence studies of oxygen-related defects in aluminum nitride, J. Am. Ceram. Soc. 73 (1990) 3238–3246, https://doi.org/10.1111/j.1151-2916.1990.tb06444.x.
[17] S. Schweizer, U. Rogulis, J.-M. Spaeth, L. Trinkler, B. Berzina, Investigation of oxygen-related luminescence centres in AlN ceramics, Phys. Stat. Sol.(b) *219* (No. 1) (2000) 171–180, https://doi.org/10.1002/1521-3951(200005)219:1<171::AID-PSSB171>3.0.CO;2-0, 2000.
[18] J.C. Nappe, M. Benabdesselam, Ph Grosseau, B. Guilhot, Effect of swift heavy ion irradiations in polycrystalline aluminum nitride, Nucl. Instrum. Methods Phys. Res. B *269* (No. 2) (2011) 100–104, https://doi.org/10.1016/j.nimb.2010.10.025.
[19] F. Karel, J. Pastrnak, J. Hejduk, V. Losik, Fine structure of emission spectra of the red AlN:Mn luminescence, Phys. Stat. Sol.(b) 15 (No. 2) (1966) 693–699, https://doi.org/10.1002/pssb.19660150230, 1966.
[20] M. Benabdesselam, P. Iacconi, D. Lapraz, P. Grosseau, B. Guilhot, Thermoluminescence of AlN – influence of synthesis processes, J. Phys. Chem. 99 (No. 25) (1995) 10319–10323, https://doi.org/10.1021/j100025a038, 1995.
[21] A. Sato, K. Azumada, T. Atsumori, K. Hara, Characterization of AlN:Mn thin film phosphors prepared by metalorganic chemical vapor deposition, J. Cryst. Growth 298 (2007) 379–382, https://doi.org/10.1016/j.jcrysgro.2006.10.042.
[22] H.-S. Do, S.-W. Choi, S.-H. Hong, Blue-emitting AlN:Eu^{2+} powder phosphor prepared by spark plasma sintering, J. Am. Ceram. Soc. 93 (2010) 356–358, https://doi.org/10.1111/j.1551-2916.2009.03424.x.
[23] L.J. Yin, Q.Q. Zhu, W. Yu, L.Y. Hao, X. Xu, F.C. Hu, M.H. Lee, Europium location in the AlN: Eu green phosphor prepared by a gas-reduction-nitridation route, J. Appl. Phys. 111 (2012), 053534, https://doi.org/10.1063/1.3692810.
[24] D.M. Spiridonov, D.V. Chaikin, N.A. Martemyanov, A.S. Vokhmintseva, I. A. Weinstein, Specific features of spectrally resolved thermoluminescence in UV-Irradiated aluminum nitride microcrystals, Opt Spectrosc. 128 (Nr 9) (2020) 1430–1432, https://doi.org/10.1134/S0030400X20090210.
[25] R. Schwarz, M. Niehus, S. Koynov, L. Melo, J. Melo, S. Cardoso, P.P. Freitas, Pulsed sub-band-gap photoexcitation of AlN, Diam. Relat. Mater. 10 (2001) 1326–1330, https://doi.org/10.1016/S0925-9635(00)00578-1.
[26] F. Liu, L. Li, T. Guo, H. Gan, X. Mo, J. Chen, S. Deng, N. Xu, Investigation on the photoconductive behaviours of an individual AlN nanowire under different excited lights, Nanoscale Res. Lett. 7 (2012) 454, https://doi.org/10.1186/1556-276X-7-454.
[27] K. Teker, J. Otto, A. Siemann, Photoconductivity of catalyst-free grown aluminum nitride nanowires, Proc. SPIE 8766 (2013), https://doi.org/10.1117/12.2016767, 9766OA-1.
[28] C. Xie, X.-T. Lu, X.-W. Tong, Z.-X. Zhang, F.-X. Liang, L. Liang, L.-B. Luo, Y.-C. Wu, Recent progress in solar-blind deep ultraviolet photodetectors based on inorganic ultrawide bandgap semiconductors, Adv. Funct. Mater. 29 (2019), 1806006, https://doi.org/10.1002/adfm.201806006.
[29] B. Berzina, L. Trinkler, V. Korsaks, R. Ruska, Nitrogen vacancy type defect luminescence of AlN nanopowder, Opt. Mater. 108 (2020), 110069, https://doi.org/10.1016/j.optmat.2020.110069.
[30] Q. Zhou, Z. Zhang, H. Li, S. Golovinskyi, X. Tang, H. Wu, J. Wang, B. Li, Below bandgap photoluminescence of an AlN crystal: Co-existence of two different charging states of a defect center, Apl. Mater. 8 (2020), 081107, https://doi.org/10.1063/5.0012685.
[31] K. Kojima, G. Okada, K. Fukuda, T. Yanagida, Influence of SrF_2 doping in AlN Ceramics on scintillation and dosimeter properties, Radiat. Meas. 94 (2016) 78–82, https://doi.org/10.1016/j.radmeas.2016.09.008.
[32] T. Yanagida, Y. Fujimoto, N. Kawaguchi, S. Yanagida, Dosimeter properties of AlN, J. Ceram. Soc. Jpn. 121 (2013) 988–991, https://doi.org/10.2109/jcersj2.121.988.
[33] K. Genji, T. Uchino, Time-resolved photoluminescence characterization of oxygen-related defect centers in AlN Appl, Phys. Lett. 109 (2016), 021113, https://doi.org/10.1063/1.4958891.
[34] A.S. Vokhmintsev, I.A. Weinstein, D.M. Spiridonov, Afterglow in bulk AlN single crystals under β-irradiation, J. Lumin. 132 (2012) 2109–2113, https://doi.org/10.1016/j.jlumin.2012.03.066.
[35] D.J. Huntley, An explanation of the power-law decay of luminescence, J. Phys. Condens. Matter 18 (2006) 1359, https://doi.org/10.1088/0953-8984/18/4/020.
[36] J. Pastrňák, J. Oswald, F. Karel, Z. Khás, Study of luminescence kinetics of AlN:Mn^{4+} under volume. Photo-excitation and surface excitation in plasma discharge, Phys. Stat. Sol. (a) 62 (1980) 341–349, https://doi.org/10.1002/pssa.2210620140.
[37] I.V. Baklanova, V.N. Krasilnikov, A.P. Tyutyunnik, A.N. Enyashin, YaV. Baklanova, O.I. Gyrdasova, R.F. Samigullina, E.G. Vovkotrub, Synthesis, spectroscopic and luminescence properties of Ga–doped γ–Al2O3, Spectrochim. Acta Mol. Biomol. Spectrosc. 227 (2020), 117658, https://doi.org/10.1016/j.saa.2019.117658.